

# Lab on a Chip

Accepted Manuscript



This is an *Accepted Manuscript*, which has been through the Royal Society of Chemistry peer review process and has been accepted for publication.

*Accepted Manuscripts* are published online shortly after acceptance, before technical editing, formatting and proof reading. Using this free service, authors can make their results available to the community, in citable form, before we publish the edited article. We will replace this *Accepted Manuscript* with the edited and formatted *Advance Article* as soon as it is available.

You can find more information about *Accepted Manuscripts* in the [Information for Authors](#).

Please note that technical editing may introduce minor changes to the text and/or graphics, which may alter content. The journal's standard [Terms & Conditions](#) and the [Ethical guidelines](#) still apply. In no event shall the Royal Society of Chemistry be held responsible for any errors or omissions in this *Accepted Manuscript* or any consequences arising from the use of any information it contains.

1 Analysis of fast protein phosphorylation kinetics in single cells on a  
2 microfluidic chip

3 Matthias Blazek<sup>1,2</sup>, Tomas Silva Santisteban<sup>1,2</sup>, Roland Zengerle<sup>2,3</sup>, Matthias Meier<sup>1,2,\*</sup>

4  
5 <sup>1</sup>Microfluidic and Biological Engineering, Department of Microsystems Engineering - IMTEK,  
6 University of Freiburg, Georges-Koehler-Allee 103, 79110 Freiburg, GERMANY

7 <sup>2</sup>Centre for Biological Signalling Studies - BIOS, University of Freiburg, GERMANY

8 <sup>3</sup>Laboratory for MEMS Applications, Department of Microsystems Engineering - IMTEK,  
9 University of Freiburg, GERMANY

10 \* Correspondence should be addressed to: matthias.meier@imtek.de

11

12 **Abstract**

13 In the present study, we developed a microfluidic large-scale integration (mLSI) platform for  
14 the temporal and chemical control of cell cultures to study fast kinetics of protein  
15 phosphorylation. For *in situ* protein analysis the mLSI chip integrates the Proximity Ligation  
16 Assay (PLA). To investigate cell-signaling events with a time resolution of a few seconds we  
17 first engineered and optimized the fluidic layout of the chip with 128 individual addressable  
18 cell culture chambers. The functionality of the cell culture operations and PLA is  
19 demonstrated by the determination of the minimum cell sample size for obtaining robust  
20 quantitative PLA signals at the single-cell level. We show that at least 350 cells per assay  
21 condition are required to statistically evaluate single cell PLA data. In the following we used  
22 the PLA chip with over 500 hundred cells per condition to record sequential phosphorylation  
23 reactions of the canonical protein kinase within the Akt pathway, which is activated in various  
24 human cancer types. This was achieved by stimulating mouse fibroblast cell cultures with  
25 either the platelet-derived growth factor (PDGF) or insulin-like growth factor (IGF-1). Fluidic  
26 cell stimulation pulses of 5 seconds were followed by precisely time shifted cell fixation  
27 pulses to obtain a temporal resolution of 10 seconds. PLA was then performed on all fixed  
28 arrays of cell cultures to extract the characteristic phosphorylation times at the single cell  
29 level for either the PDGF, or IGF-1 receptor and the Akt and GSK3 $\beta$  kinases. Characteristic  
30 phosphorylation times for the receptors were between 13 and 35 seconds, whereas for  
31 downstream kinases between 25 and 200 seconds. Thus we could reveal a molecular order  
32 of the phosphorylation reactions during the signal transduction through the Akt pathway. In  
33 dependence of the stimulus we found a temporal difference for the characteristic  
34 phosphorylation time of 20 and 150 seconds for the Ser-473 and Thr-308 residues on the Akt  
35 kinase, respectively. Temporal alteration of sequential phosphorylation reactions on Akt has  
36 been proposed as molecular mechanism to differentiate between stimuli and biophysically  
37 determined in the present study.

38

39

## 1 Introduction

2 Cells are information-processing devices. A predominant molecular mechanism for  
3 transferring signals from the extracellular microenvironment to the inner compartments of  
4 cells governs the sequential transfer and removal of phosphorus groups from proteins<sup>1</sup>.  
5 Kinases and phosphatases are proteins that catalyze the phosphorylation and reverse de-  
6 phosphorylation reaction, respectively. Approaches for screening large-scale protein  
7 phosphorylation reactions,<sup>2,3</sup> in combination with individual protein characterization studies,  
8 have led to the construction of complex physical maps of the phosphorylation network<sup>4</sup>,  
9 involving the connections between kinases, phosphatases, and their substrates. Despite the  
10 high availability of phosphorylation data, our current understanding about the signal  
11 transduction remains static. One reason for this is the lack of quantitative detection  
12 technologies for probing protein phosphorylation in single cells with high sensitivity,  
13 specificity, and throughput.

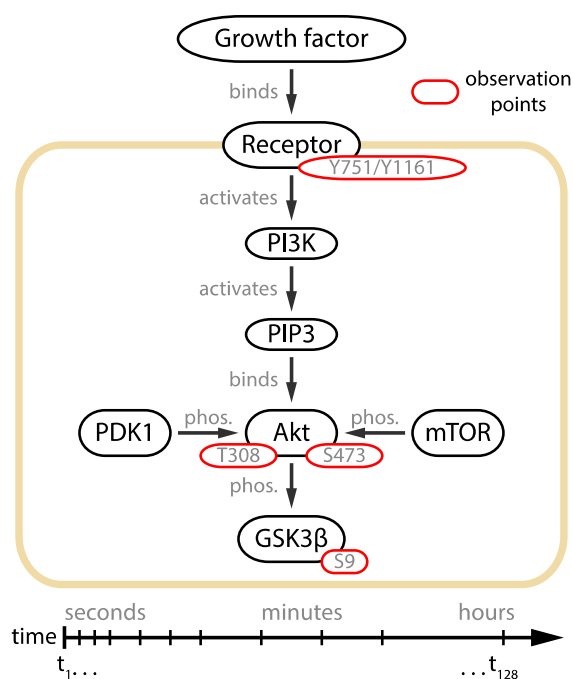
14 Recent advances of standard protein phosphorylation assay technologies, for  
15 example, western blotting analysis, mass spectrometry, and fluorescence-activated cell  
16 sorting (FACS) technique, start to fill this technical gap. An example of this progress is the  
17 miniaturization of the classical western blot assay onto a microfluidic chip<sup>5</sup>, which leads to an  
18 increase in sensitivity and thus widens the scope of applications for analysis of single cells<sup>6</sup>.  
19 Despite these promising advances, to obtain quantitative protein phosphorylation data still  
20 remains a challenge. More importantly, none of the existing techniques offer the temporal  
21 resolution required for characterizing the fast kinetics of protein phosphorylation reactions.  
22 This is due to an interrupted technical workflow between the sample preparation and protein  
23 analytical assay. Phosphorylation reactions in response to a cell stimulus occur in the  
24 second-to-minute time regime.<sup>7</sup> Manually performed *in situ* cell experiments with standard  
25 flasks have reliable time resolutions of only one minute. Furthermore, the low number of  
26 repeats gives rise to large variances in the *in situ* experiments.

27 An alternative assay technology for quantifying proteins, their interactions, and  
28 posttranslational modifications is proximity ligation assay (PLA)<sup>8,9</sup>. PLA is an immuno-based  
29 assay, in which two oligonucleotide-labeled antibodies (Ab's) are primed to the same target  
30 at different epitopes. The proximity of the two Ab's is tested by a hybridization reaction of the  
31 oligonucleotide labels. A circular DNA template between the antibody labels and two  
32 additional oligonucleotide strands is formed. The circular DNA template is ligated and  
33 amplified by isothermal rolling circle amplification. As a result, a DNA polymer with a  
34 diameter of about 0.5  $\mu\text{m}$  is generated at the cellular location of the protein event. The DNA  
35 polymer is stained with a fluorescent probe molecule. Although the *in situ* technology offers  
36 high sensitivity and specificity paired with cellular localization information, its throughput is  
37 severely limited by the complexity of the biochemical steps and end-point detection mode.

38 To overcome these drawbacks and to enable the PLA technology to quantify the  
39 protein phosphorylation dynamics, we integrated the PLA approach onto a chip in the  
40 previous study<sup>10</sup>. The microfluidic large-scale integration<sup>11</sup> (mLSI) technique combined the  
41 PLA platform with an array of independent cell culture chambers. The microchambers  
42 containing the cell cultures were arranged in a matrix format and allowed the screening of  
43 two independent parameters such as stimulation time and protein targets in PLA, in one *in*  
44 *situ* cell signaling experiment. Although the first-generation PLA platform could reveal the  
45 dynamics of protein phosphorylation in response to a cell stimulus, its quantification

1 performance was hampered by low cell count statistics and a low time resolution of a few  
2 minutes.

3 Herein, we designed and engineered an mLSI platform consisting of individually  
4 addressable cell culture chambers in a serial configuration by using polydimethylsiloxane  
5 (PDMS). Different from the first PLA chip, the new mLSI chip was designed and optimized for  
6 tracing the response kinetics of protein phosphorylation events in the order of seconds. To  
7 demonstrate the advances in automation, miniaturization, and parallelization of the chip, we  
8 resolved the phosphorylation kinetics of four phosphorylation sites within the Akt signaling  
9 pathway upon the cell stimulation with different growth factors. The observed protein  
10 phosphorylation targets and their positions in the signaling cascade are summarized in  
11 **Figure 1**. Of particular interest in this study is the double phosphorylation of the Akt kinase,  
12 which is an eponymous element of the pathway. The activation of the Akt kinase is a  
13 hallmark for several types of human cancer.<sup>12,13</sup> It has been shown that the full activation of  
14 Akt kinase requires the phosphorylation of its residues Ser-473 and Thr-308.<sup>14</sup> The temporal  
15 order of Akt phosphorylation remains a long-standing research question.<sup>15-17</sup> The time traces  
16 of the Akt kinase phosphorylation recorded by the PLA chip in this study settled this question  
17 and enabled the application of this strategy for high-content cell-signaling studies.



18

19 **Figure 1.** Illustration of the Akt signal transduction pathway<sup>14</sup>. Extracellular signals are  
20 transmitted to the interior of the cell by a protein phosphorylation cascade starting at the cell  
21 membrane receptor. The substrate binding leads to the auto-phosphorylation of the receptor  
22 protein and activation of its kinase function. In the case of PDGF and IGF-1 receptors, the  
23 residues Tyr-751 and Tyr-1161 are auto-phosphorylated, respectively. The phosphorylation  
24 signal is passed to the phosphatidylinositol 3 kinase (PI3K), which produces  
25 phosphatidylinositol (3,4,5)-triphosphate (PIP3) at the inner surface of the cell membrane. In  
26 the following steps, Akt is recruited to the membrane and phosphorylated at its residues Thr-  
27 308 and Ser-473, by the kinases PDK1<sup>18</sup> and mTOR<sup>16</sup>. Upon double phosphorylation, the  
28 kinase domain of Akt gains full activity and distributes the signal downstream to over a  
29 hundred substrates<sup>14</sup>, where GSK3β is one of them<sup>19</sup>. Yellow, black, and red enclosures  
30 indicate the cell membrane, proteins, and their phosphorylation sites, respectively.

## 1 **Experimental**

### 2 *Chip fabrication*

3 PDMS chips were manufactured using the standard soft lithography methods<sup>20</sup> for two-layer  
4 devices<sup>11</sup>. Briefly, SU-8 3050 (MicroChem) and AZ 40 XT photoresists (MicroChem) were  
5 used for fabricating the molds of the cell culture chambers and connecting channel network  
6 in the flow layer, respectively. The mold for the control channels was fabricated by using SU-  
7 8 3025 (MicroChem). All features on the molds were 25  $\mu\text{m}$  in height, except the cell culture  
8 chambers, which were 50  $\mu\text{m}$  high. Chips were replicated from the molds by using Sylgard  
9 184 PDMS (Dow Corning). The flow and control layers were bonded together using an off-  
10 ratio procedure. Pneumatic membrane valves of the chip were constructed in a pushdown  
11 configuration. In a final step the assembled PDMS chip was bonded to a glass carrier (Brain  
12 Laboratories) through oxygen plasma activation.

### 13 *Chip operation*

14 The PDMS chips were mounted inside an on-stage microscopic cell incubator. Cell culturing  
15 media and buffers were stored in glass containers and supplied to the chip through Tygon  
16 tubings (Saint-Gobain). Assay reagents or water for the control channels were stored in  
17 Tygon tubings, which were directly inserted into the chip. All control and flow lines were  
18 separately pressurized via a solenoid valve at 200 and 40 kPa, respectively. A graphical user  
19 interface (GUI) within the Matlab programming environment (Mathworks) was used for  
20 automating the opening and closing cycles of the solenoid valves and for activating either the  
21 on-chip pneumatic membrane valves or the flow of the assay reagents.

### 22 *Cell culture*

23 NIH3T3 mouse fibroblast cells (DMSZ) were cultured off-chip in high-glucose Dulbecco's  
24 modified Eagle's medium (DMEM) supplemented with 10% fetal bovine serum (FBS) and 1%  
25 PenStrep (all from Life Technologies) by following the standard procedures (ATCC). Cells  
26 were harvested and re-suspended at a concentration of  $5 \times 10^6$  cells/ml. Before seeding the  
27 cell suspension, all cell culture chambers in the PDMS chip were coated with a fibronectin  
28 (Sigma Aldrich) solution of 0.05%. Cells were cultured on-chip with full medium in a 5%  $\text{CO}_2$   
29 atmosphere at 37°C for 6 h and then starved under low-FBS conditions, i.e., 0.1% FBS, for  
30 12 h. Medium exchange at every 90 min was automated by the protocols through the Matlab  
31 GUI. Cells were stimulated with platelet-derived growth factor PDGF-BB (Prospec  
32 Technogene) or insulin-like growth factor IGF-1 (Sigma Aldrich) at a concentration of 100  
33 ng/ml or 200 ng/ml, respectively. Both growth factors were diluted with cell starvation  
34 medium. After stimulation, the cells were fixed with 4% formaldehyde (ThermoFisher  
35 Scientific) for 16 min at room temperature and permeabilized with 0.05% Tween 20 (Sigma  
36 Aldrich) for 3 min.

### 37 *On-chip Proximity Ligation Assay*

38 Fixed cells were blocked (Olink) on-chip for 1 h. Next, monoclonal primary antibodies (Cell  
39 Signaling Technology) were diluted with antibody diluent (Olink) and incubated with the cell  
40 samples for 12 h with refresh cycles repeated every 2 h. The dilution ratio was 1:50 for Akt  
41 (Ser-473) (Cell Signaling, 4060), Akt (Thr-308) (Cell Signaling, 2965), and GSK-3 $\beta$  (Ser-9)  
42 (Cell Signaling, 9323), 1:25 for the PDGF  $\beta$  receptor (Tyr-751) (Cell Signaling, 3161), and  
43 1:250 for the IGF-1 receptor (Tyr-1161) (Santa Cruz Biotechnology). Anti-rabbit PLA probes

1 (anti-rabbit Plus and Minus, Olink) were diluted with Duolink antibody diluent at a ratio of 1:5  
2 and incubated at room temperature for 2 h. DNA connectors (Olink) with the T4 ligase  
3 (Fermentas) were incubated at 32°C for 1 h. Amplification reagents (Olink) were diluted  
4 according to the vendor's instructions and incubated at 32°C for 2 h. Cell nuclei and  
5 cytoskeletons were counterstained with 4',6-diamidino-2-phenylindole dihydrochloride (DAPI)  
6 (Sigma Aldrich) and Phalloidin-Atto 488 (Sigma Aldrich), respectively.

#### 7 *Automation of the chip workflow*

8 Two consecutive and automated protocols were developed for performing the cell stimulation  
9 experiments coupled with the PLA process. The on-chip valve configuration and flow  
10 pressure in each step was activated with the aid of a multichannel pressure-control system<sup>21</sup>  
11 equipped with solenoid valves and a programmable interface. The flow pressure was fixed to  
12 40 kPa in all following stimulation experiments. The first protocol included the steps: (1)  
13 coating of the glass channel surface with fibronectin, (2) cell seeding and culturing, (3)  
14 serum-starvation of the cells, (4) growth factor stimulation, and (5) cell fixation. The protocol  
15 consisted of 3200 automated flush steps completed over a period of 18 h. After the fixation of  
16 cells, the second protocol, including all PLA steps, was executed as follows: (6) cell  
17 permeabilization, (7) antigen blocking, (8) target detection with DNA-labeled antibodies, (9)  
18 ligation of the circular DNA template, (10) rolling circle amplification, and (11) fluorescence  
19 staining. The second protocol contained 3600 flush steps executed over a time period of 18  
20 h. The detailed flush cycles, times, and temperatures are summarized in SI table 1, whereas  
21 the reagent compositions are given above.

#### 22 *Image acquisition and analysis*

23 Fluorescent images were acquired using the Axio Observer inverted microscope equipped  
24 with a 20× Plan Aplanachromat objective, AxioCam MRm camera, and Zen microscope  
25 software (all from Zeiss). Images were taken at eight positions in each cell culture chamber;  
26 and the filter sets of 43HE, 38HE, and 49 were used for the fluorescently stained PLA dots,  
27 cytoskeletons, and nuclei, respectively. The integration times were constant over the entire  
28 imaging procedure. The image analysis process, including cell segmentation and PLA dot  
29 identification, was performed by using Matlab image processing toolbox (Mathworks).

30

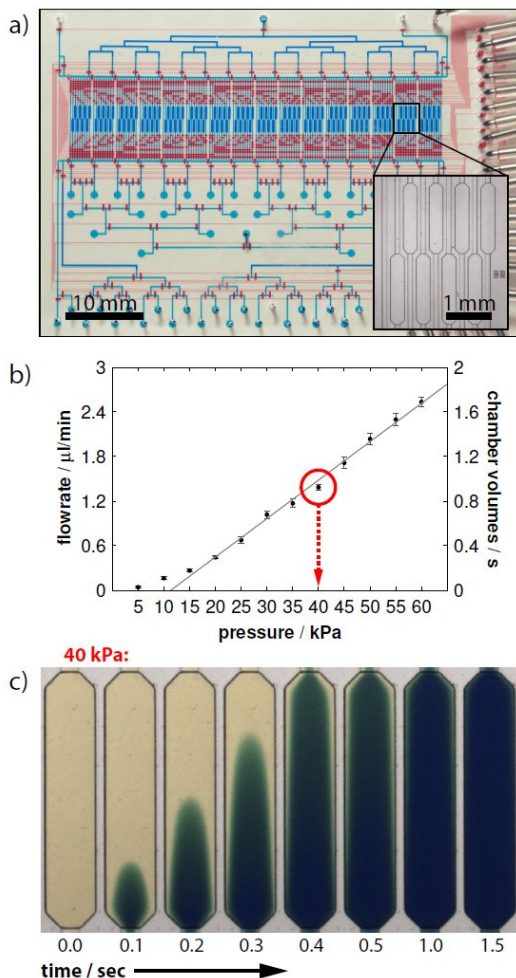
## 31 **Results**

#### 32 *Microfluidic large-scale integration platform*

33 The design of the mLSI chip with PLA functionality for recording *in situ* protein  
34 phosphorylation reactions is illustrated in **Figure 2a**. The two-layer PDMS chip was  
35 manufactured by a rapid prototyping procedure.<sup>20</sup> In the lower PDMS layer, a fluidic channel  
36 network addresses the 128 parallel-arranged cell culture chambers (blue). Each  
37 microchamber occupies an area of 0.5 mm<sup>2</sup> and volume of 25 nl. The microchambers are  
38 organized into 16 logic blocks, and each consists of 8 chambers (**Figure 2a** inset). Fluids  
39 were routed from the multiplexed inlet ports to individual cell culture chambers by 1622  
40 pneumatic membranes valves. The corresponding control channel network was implemented  
41 into the top PDMS layer. The assembled PDMS chips were bonded to a glass carrier, which  
42 concomitantly provided the functional substrate for cell cultures.

1 The theoretical time resolution for an on-chip cell stimulation experiment is given by  
 2 the volume exchange time of one cell culture chamber. Therefore, we measured the rate of  
 3 volume flow through the PLA chip in dependence of the applied flow pressure. During the  
 4 measurements, the fluid was directed from the inlet ports through the channel network and  
 5 one cell culture chamber to the outlet port. The expected linear dependence of volume flow  
 6 rates (left axis) and applied flow pressures is shown in **Figure 2b**. Error bars indicate one  
 7 standard deviation from six independent experiments performed in different cell culture  
 8 chambers. With the given volume of one cell culture chamber (25 nl), we calculated the  
 9 volume exchange rate of one cell culture chamber and exchange time (in seconds) at  
 10 different applied flow pressures (right axis). The exchange time of one chamber volume was  
 11 one second at a flow pressure of 40 kPa. We further confirmed this value by performing time-  
 12 lapse imaging of a cell culture chamber by using colored aqueous solutions. As shown in  
 13 **Figure 2c**, the fluid stream flowing through the chamber exhibited the characteristic  
 14 Poiseuille flow profile from the time points of 0.1 s to 1.0 s. After 1.5 s, the fluid near the  
 15 chamber side walls was completely stained and showed no difference in color intensity from  
 16 the center region. The fluidic resistance from the inlet ports through each cell culture  
 17 chamber to the outlet port was designed to be equal. Because the cell stimulation experiment  
 18 with the subsequent cell fixation process requires the operation of two fluid routes, the  
 19 highest achievable time resolution is therefore twice that of the volume exchange rate.

20



21

1 **Figure 2.** Microfluidic PLA-Chip design and fluid characterization. a) Layout of the fluidic  
 2 chip. For the purpose of illustration, the microchannels of the control and flow layers are filled  
 3 with red and blue aqueous solutions, respectively. The entire device covers an area of  $65 \times$   
 4  $48 \text{ mm}^2$ , within which the 128-cell culture chambers constitute the central elements. Scale  
 5 bar denotes 10 mm. Inset: Zoomed-in view of the microchambers for cell cultures. Scale bar  
 6 denotes 1 mm. b) Plot of the volume flow rate from one inlet port through a cell culture  
 7 chamber to the outlet against the applied flow pressure. A flow pressure of 40 kPa ensures  
 8 the exchange of about one cell chamber volume (25 nl) within 1 s. c) Time-lapsed image  
 9 series of colored aqueous solution streaming through one cell culture chamber at an applied  
 10 flow pressure of 40 kPa.

11

### 12 *Statistics for robust single-cell PLA analysis*

13 One of the advantages of the PLA technology is its ability to produce inherent single cell  
 14 information. Single-cell information gives insight into the biological cell-to-cell variability,  
 15 which is especially useful for the characterization of heterogeneities and robustness of  
 16 signaling transduction.<sup>22,23</sup> Quantitative protein information from single cells can be obtained  
 17 through image analysis process, including cell segmentation, PLA dot identification, and dot-  
 18 assignment to cell areas. However, the number of cells that are sampled with PLA dots for  
 19 obtaining reproducible and statistically reliable single-cell PLA results remains unclear. From  
 20 the engineering point of view, this number also concomitantly delimits the minimum size for  
 21 the cell culture chamber.

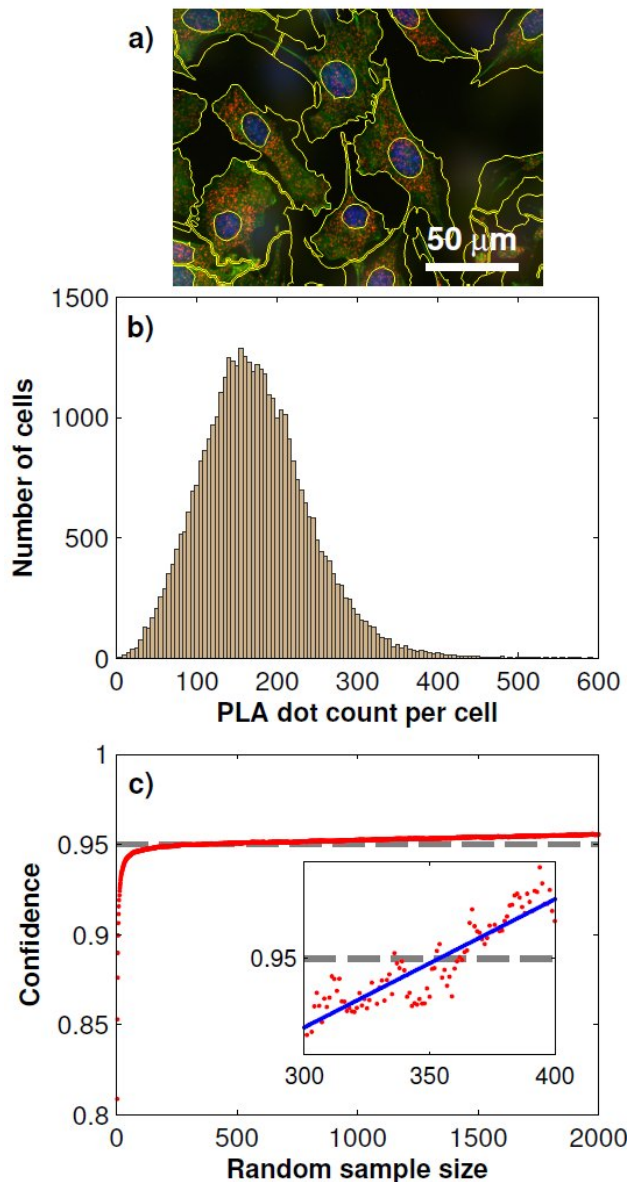
22 We addressed this question by systematically evaluating a large sample of mouse  
 23 fibroblast cells (NIH-3T3) cultured in all 128 microchambers. Each chamber was seeded with  
 24 about 400 cells, which, on average, covered 40% of the microchamber surface. Before  
 25 fixation, cells were stimulated with 200 ng/ml IGF-1 for 10 min on-chip. IGF-1 triggered the  
 26 Akt phosphorylation cascade. During the following PLA analysis, we targeted the Thr-308  
 27 phosphorylation site of Akt in all cells. A total number of 1024 microscopic images were  
 28 acquired and analyzed for extracting the single-cell PLA dot distributions. **Figure 3b** shows  
 29 the distribution of the PLA dot counts of the phosphorylated Akt measured with more than  
 30 40,000 cells. The mean PLA dot count per cell was

31 To determine the minimum cell sample size for obtaining a robust on-chip PLA result,  
 32 we performed a Monte Carlo simulation, which generated random sub-samples of the full  
 33 data set. For each sub-sample, the arithmetic mean value, standard deviation, and 95%  
 34 confidence interval,  $I_C^{95}$ , of the PLA result can be calculated by using the following equation:

$$I_C^{95} = \left[ \mu - q_{0.025} \cdot \frac{\sigma}{\sqrt{n}}; \mu + q_{0.975} \cdot \frac{\sigma}{\sqrt{n}} \right]$$

35 where  $\mu$  is the arithmetic mean value,  $\sigma$  is the standard deviation,  $n$  is the number of cells,  
 36 and  $q_{0.025}$  and  $q_{0.975}$  are the quantiles of 2.5% and 97.5%, respectively. Each confidence  
 37 interval against the “true” PLA mean value of the full cell sample set was analyzed by a  
 38 hit/miss test. In total, 4 million random sub-samples with sizes between 2 and 2000 single  
 39 cells were analyzed. The corresponding plot of the randomized cell sub-samples against the  
 40 confidence value of the hit/miss test is shown in **Figure 3c**. It was found that 95% of the sub-  
 41 samples with  $n > 350$  passed the hit/miss test. This value is regarded as the minimum cell  
 42 sample size for on-chip PLA experiments targeting the Akt Thr-308 phosphorylation site.





1

2 **Figure 3.** Statistical evaluation of the minimum cell sample size required for robust single-cell  
 3 PLA results. a) Exemplary image of PLA results and single cell segmentation. b) PLA dot  
 4 count distribution for the phosphorylated Akt at the Thr-308 residue obtained from 40,000  
 5 single cells cultured under the same conditions. c) Monte Carlo simulation of the 95%  
 6 confidence interval for different sample sizes. The current statistical setup indicates a  
 7 recommended sample size of at least 350 cells per assay.

8 The minimum cell sample size depends on the absolute PLA dot count numbers per cell,  
 9 which in turn is a function of the antibody concentration, affinity, incubation time, and/or  
 10 fixation method used in the PLA experiment. To obtain a more general result for the minimal  
 11 cell sample size we repeated the above analysis for four different protein targets in its  
 12 phosphorylation state. The results are summarized in Table 1. It can be observed that with  
 13 decreasing mean PLA dot count per cell the minimum cell sample size is increasing. At the  
 14 lowest tested mean PLA dot count of 33 the minimum cell sample size was 470. At a cell  
 15 confluency of 80%, about 800 fibroblast cells can be cultured in each of the 128  
 16 microchambers, and this number exceeds about twice the amount required for achieving the  
 17 95% confidence interval for single-cell PLA experiments.

1 Table 1. Calculated minimum cell sample size for different phosphorylation targets

Antibody Target	Cell Sample Size	PLA dots/cell	95% confidence level
Akt Thr-308	40000	172 ± 76	350
Akt Ser-473	24000	113 ± 58	320
GSK3β Ser-9	18000	140 ± 66	290
PDGFR Tyr-751	30000	33 ± 17	470

2

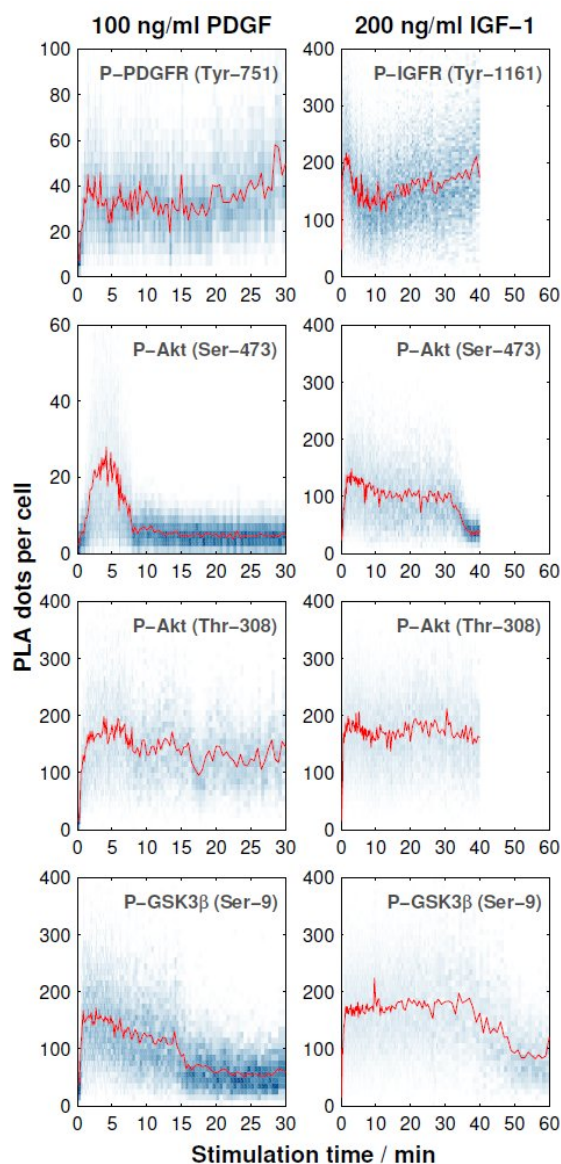
3

4 *Fast phosphorylation kinetics of the Akt signaling pathway*

5 In the next step, we recorded the phosphorylation kinetics of the Akt pathway at four  
6 observation points (see **Figure 1**) upon cell stimulation with the growth factors PDGF and  
7 IGF-1. The phosphorylation rates of the receptors depend on the amount of growth factors in  
8 the microenvironment.<sup>24,25</sup> Half-maximum activation concentrations ( $EC_{50}$ ) for the  
9 phosphorylation reaction of both PDGF and IGF-1 receptors are reported to be between 1  
10 ng/ml and 10 ng/ml.<sup>24-27</sup> The downstream phosphorylation reactions of Akt are reported to be  
11 saturated at PDGF and IGF-1 concentrations of about 30 ng/ml and 75 ng/ml, respectively.  
12<sup>28,29</sup> For comparing the phosphorylation kinetics triggered by the two growth factors, cells  
13 were stimulated with a growth factor three times higher than the signal saturation  
14 concentration of the hormones.

15 Next, we exploited the cell culture chambers in the PLA chip to generate a time  
16 trajectory for one protein phosphorylation reaction. To achieve this, the cultured cells were  
17 starved with a serum-free media (0.1% FBS) for 12 h and then stimulated with a fluid pulse  
18 containing the growth factor. The fixation of the cells at different time points after stimulation  
19 maintained the molecular signaling response within the cells. We recorded the response with  
20 a time resolution of 10 s during the first 8 min after stimulation, from which onwards the time  
21 gap was increased to cover a time-frame between 30 min and 60 min depending on the  
22 protein target. The array of 128 fixed cell cultures was then subjected to the PLA assay. The  
23 automated imaging process and image analysis resulted in the time trajectories of single-cell  
24 PLA dot count distributions, as shown in **Figure 4**.

25



1

2

3

4

5 **Figure 4.** Time trajectories of single-cell PLA dot count distributions for the evaluation of  
 6 protein phosphorylation kinetics. Left columns show the phosphorylation kinetics of the  
 7 PDGF receptor and three kinases within the Akt pathway upon PDGF stimulation, and right  
 8 columns represent the phosphorylation kinetics of the IGF-1 receptor and three kinases  
 9 within the Akt pathway upon IGF-1 stimulation. Each time point shown in the graphs  
 10 represents the normalized PLA dot count distributions (blue, in y-direction) evaluated from  
 11 more than 400 single cells. Mean values are indicated in red.

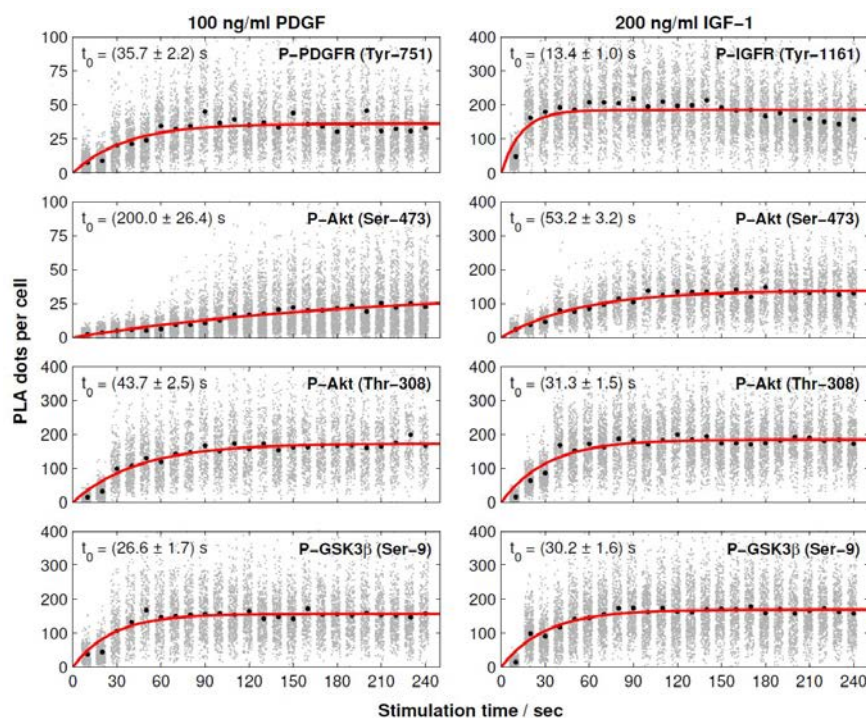
12

13 We observed an increase in the mean value (red line in Figure 4) of the single-cell  
 14 PLA dot count (blue dots along the vertical direction shown in Figure 4) of all phosphorylation  
 15 targets in response to the stimuli. The duration of the PLA dot count increase varied among

1 the targets. PLA signal for both receptors and the Thr-308 residue of Akt did not return to the  
2 basal levels within the observation period. A response difference between the two growth  
3 factors was observed during the increase of the PLA signal of Akt at Ser-473 and GSK3 $\beta$  at  
4 Ser-9. As expected, the PLA signal of GSK3 $\beta$ , which is a substrate of Akt, decreases after  
5 the PLA signal of Akt in both cases.

6 To quantify the phosphorylation rates of the proteins, all single-cell PLA dot count  
7 distributions, up to the first 240 s, were fitted into a first order rate equation:  $N(t) = a \cdot (1 -$   
8  $e^{-\frac{t}{t_0}})$ , with  $N(t)$ ,  $a$ ,  $t$ , and  $t_0$  denoting the PLA dot count distribution, a constant, the time, and  
9 characteristic phosphorylation time, respectively. The temporal PLA dot count distributions  
10 and fitting results are shown in **Figure 5**. As expected, the receptor kinases exhibit the  
11 fastest characteristic phosphorylation time among all pathway components, and the  
12 characteristic phosphorylation time of IGF-1 ( $t_0 = 13.6 \pm 1$  s) is three times larger than that of  
13 PDGF ( $t_0 = 35.6 \pm 2.2$  s). In addition, the phosphorylation reactions of the two Akt residues in  
14 response to the IGF-1 stimulation are faster than that in response to the PDGF stimulation.  
15 The comparison of the characteristic phosphorylation times revealed a difference between  
16 the two monitored residues of Akt upon stimulation with IGF-1 and PDGF. In both cases, the  
17 characteristic phosphorylation time of the Thr-308 residue was faster than that of the Ser-473  
18 residue. Upon PDGF stimulation the characteristic phosphorylation time of the Akt Ser-473  
19 residue ( $t_0 = 200 \pm 26.4$  s) was four times slower than the characteristic phosphorylation time  
20 of the Akt Thr-308 residue ( $t_0 = 43.7 \pm 2.5$  s). Upon IGF-1 stimulation the characteristic  
21 phosphorylation time of the Ser-473 ( $t_0 = 53 \pm 3.2$  s) was still slower than the for the Thr-308  
22 residue ( $t_0 = 31.3 \pm 1.6$  s) but the difference between the two sites was only about  $22 \pm 3$  s.

23 While the characteristic phosphorylation time of the receptors and downstream Akt  
24 kinase followed the expectation of a canonical signaling pathway was the characteristic  
25 phosphorylation time of the GSK3 $\beta$  Ser-9 residue not in accordance with the signal  
26 processing image in Figure 1. GSK3 $\beta$  is known to be a substrate of Akt. However, the  
27 present study revealed a faster characteristic phosphorylation time of the Ser-9 residue of  
28 GSK3 $\beta$  than that of Akt upon PDGF and IGF-1 stimulations. This result suggests either a  
29 strong catalytic activity of Akt towards GSK3 $\beta$  or a second kinase, which is activated faster  
30 than Akt, cross-activates the phosphorylation of GSK3 $\beta$  upon PDGF and IGF-1 stimulations.



1

2 **Figure 5.** Phosphorylation rates evaluated from the time trajectories of single-cell PLA dot  
 3 count distributions. The left and right columns represent the first 240 seconds of the protein  
 4 phosphorylation time trajectories upon PDGF and IGF-1 stimulations, respectively. PLA dot  
 5 counts of single cells are shown in gray. The mean values of the PLA dot counts are  
 6 indicated by black dots. The simulated phosphorylation dynamics are shown in red.

7

## 8 Discussion

9 Akt pathway plays an important role in central cellular signaling transduction for the control of  
 10 cell growth, apoptosis, and various metabolic processes. High-resolution kinetics of the Akt  
 11 signal transduction next to quantitative data are missing but required for our understanding  
 12 and prediction of cellular signal processing. In the present study, we developed a microfluidic  
 13 tool with PLA functionality and demonstrated its capability for providing biophysical  
 14 parameters for investigating the cell signaling dynamics.

15 The minimum cell sample size to obtain reproducible phosphorylation signals with the  
 16 on-chip PLA technology is in the order of 400 cells. This value provides an initial reference to  
 17 all PLA studies, whereas, it could be modified according to the protein target, antibody, and  
 18 number of dot count observed from the cells. Several hundreds to one thousand cell repeats  
 19 have been previously used for obtaining statistically robust results from fluorescence *in situ*  
 20 hybridization (FISH) experiments<sup>30-32</sup>, and these should be in principle similar to the PLA  
 21 experiments, which are also based on a fluorescent dot-based detection method.

22 In general, kinase phosphorylation within signal transduction cascades leads to  
 23 various molecular causalities, e.g., change of kinase activity, sub-cellular location, and/or  
 24 protein interaction partners. These molecular state changes of kinases are used for directing,  
 25 distributing, and controlling the duration of signals within cells.<sup>33</sup> The complexity of molecular  
 26 events in response to a phosphorylation action led to controversial discussions regarding the  
 27 order and causalities of the molecular changes.

1 Phosphorylation kinetics with resolutions of few seconds can reveal mechanistic  
2 details of the signal transduction process. The resolutions of the phosphorylation kinetics of  
3 PDGF and IGF-1 receptors in NIH 3T3 cells are reported to be in the order of 1–2 min. With  
4 the aid of on-chip PLA technology, we quantitatively revealed the phosphorylation kinetics of  
5 both hormone receptors upon the stimulation of NIH 3T3 cells. The improved time resolution  
6 of 10 seconds in the on-chip PLA experiments resulted in a precise characteristic  
7 phosphorylation time ( $t_0 = 35 \pm 2$  s) of the PDGF receptor, whereas the accuracy of the  
8 phosphorylation rate of the IGF receptor suffered from a low resolution. Nevertheless, the  
9 time trajectories of PLA signals for the IGF-1 receptor were sufficient for predicting a fast  
10 characteristic phosphorylation time ( $t_0 = 13 \pm 1$  s) and resolving the difference between the  
11 characteristic phosphorylation times of the receptors in response to their hormones. The  
12 direct comparison of the signal transduction pathway based on the phosphorylation kinetics  
13 of the two receptors oversimplifies their functions, since both are formed upon the binding of  
14 the substrate to higher-ordered protein complexes. Thus, the characteristic phosphorylation  
15 time of the receptor is the only reliable indicator of its activity. Activation rates of the  
16 downstream kinases are dependent on the fraction of the activated receptors and therewith  
17 on the concentration of growth factors in the cellular surrounding. Within the saturation  
18 regime of the receptors with growth hormones the phosphorylation rates of the downstream  
19 kinases become independent of the growth factor concentration. The calculated  
20 characteristic phosphorylation times of all downstream kinases within the IGF-1 pathway  
21 were slower than those of the receptor kinases. In case of the PDGF pathway, however the  
22 characteristic time constant for the GSK3 $\beta$  phosphorylation is faster than for the receptor,  
23 which argues that a simple linear phosphorylation reaction model can not describe the  
24 experimental data.

25 In general, to differentiate extracellular stimuli, kinases can form specific protein  
26 complexes and phosphorylation patterns and/or change the cellular position. Two  
27 hypotheses for the molecular events of Akt in response to cell stimulation with growth factors  
28 have been proposed based on experimental results: (i) the synthesis of PIP3 leads to the  
29 recruitment of Akt into the inner leaflet of the membrane, and this facilitates the association  
30 with PDK1 and the phosphorylation of the Thr-308 residue<sup>18</sup>. Separately, the mTOR kinase  
31 complexed with the adaptor protein Rictor is activated and phosphorylates Akt at the Ser-473  
32 residue<sup>16</sup> at an undefined cellular location. (ii) Alternatively, mTOR activated in response to  
33 the growth factor stimulation phosphorylates Akt at the Ser-473 residue, followed by the  
34 binding of Akt to PIP3 and phosphorylation of the Thr-308 residue through PDK1<sup>15</sup>. It has  
35 been suggested that neither orders of the process is mutually exclusive; the prevalence of  
36 one or the other may be context-dependent<sup>17</sup>. However, *in vitro* experiments have shown that  
37 Ser-473-phosphorylated Akt led to an increase in the affinity for PDK1; thus, the sequential  
38 phosphorylation of Akt was thought to start at Ser-473, followed by Thr-308<sup>15</sup>.

39 In this study, the recorded *in situ* phosphorylation rates of the two Akt residues in  
40 response to PDGF stimulation indicate that the sequential phosphorylation of Akt starts at the  
41 Thr-308 residue, followed by Ser-473. In the case of IGF-1 stimulation, a difference between  
42 the two phosphorylation rates of Akt was observed. Although the Thr-308 residue showed a  
43 larger rate constant than that of Ser-473, their phosphorylation reactions were not temporally  
44 separated. A further indication is that the signaling through the Akt kinase pathway is  
45 regulated at the molecular level depending on the stimulus, can be deduced from the  
46 duration of the Akt phosphorylation. The Ser-473 residue is in response to IGF-1 three times  
47 longer phosphorylated than upon PDG stimulation.

1 As with GSK3 $\beta$ , which was expected to be the receiving kinase in the observed  
2 signaling cascade, the phosphorylation rate was larger than that of the proceeding kinase  
3 Akt. Apart from the Akt kinase, at least three additional kinases are reported to target the  
4 phosphorylation site Ser-9 of GSK3 $\beta$ <sup>34</sup>. One of them is MAPK, which is known to be activated  
5 in parallel to the Akt kinase upon growth factor stimulation<sup>35</sup>. A faster signal-processing  
6 through the MAPK kinase pathway than that through the Akt kinase pathway can explain the  
7 faster phosphorylation rate of GSK3 $\beta$  than that of Akt. It is worth noting that the rate constant  
8 does not exclude the possibility of phosphorylation of GSK3 $\beta$  by Akt. In fact the correlated  
9 duration of Ser-9 of GSK3 $\beta$  and Ser-473 of Akt phosphorylation upon IGF-1 and PDGF  
10 stimulations strongly indicates this and supports previous literature reports.<sup>19</sup>

11 In conclusion, the integration of highly parallel cell culture and processing  
12 performance with PLA functionality onto a microfluidic chip was successfully demonstrated  
13 by the measurement of the phosphorylation kinetics of the kinases within the Akt pathway.  
14 The variances of the PLA dot count distributions of all kinetic time traces were used for  
15 determining the kinetic rate constants. It is expected that the time trajectories of PLA dot  
16 count distributions at the single cell level can be useful for the detailed modeling of cell  
17 signaling cascades and deciphering the heterogeneities between multiple cell populations in  
18 the future.

## 19 ACKNOWLEDGEMENT

20 This study was supported by the Excellence Initiative of the German Federal and State  
21 Governments (EXC-294) and by the German Research Foundation (Emmy-Noether Grant  
22 ME3823/1-1). We thank Prof. M. Reth and G. Roth for helpful discussion.

23

## 24 REFERENCES

- 25 1. G. Burnett and E. P. Kennedy, *J Biol Chem*, 1954, **211**, 969–980.
- 26 2. M. Mann and O. N. Jensen, *Nat Biotechnol*, 2003, **21**, 255–261.
- 27 3. R. Aebersold and M. Mann, *Nature*, 2003, **422**, 198–207.
- 28 4. P. V. Hornbeck, J. M. Kornhauser, S. Tkachev, B. Zhang, E. Skrzypek, B. Murray, V.  
29 Latham, and M. Sullivan, *Nucleic Acids Res*, 2011, **40**, D261–D270.
- 30 5. A. J. Hughes and A. E. Herr, *PNAS*, 2012, **109**, 21450–21455.
- 31 6. A. J. Hughes, D. P. Spelke, Z. Xu, C.-C. Kang, D. V. Schaffer, and A. E. Herr, *Nat*  
32 *Meth*, 2014, **11**, 749–755.
- 33 7. C. Salazar and T. Höfer, *FEBS Journal*, 2009, **276**, 3177–3198.
- 34 8. S. Fredriksson, M. Gullberg, J. Jarvius, C. Olsson, K. Pietras, S. M. Gústafsdóttir, A.  
35 Ostman, and U. Landegren, *Nat Biotechnol*, 2002, **20**, 473–477.
- 36 9. O. Söderberg, K.-J. Leuchowius, M. Gullberg, M. Jarvius, I. Weibrecht, L.-G. Larsson,  
37 and U. Landegren, *Methods*, 2008, **45**, 227–232.
- 38 10. M. Blazek, C. Betz, M. N. Hall, M. Reth, R. Zengerle, and M. Meier, *Mol. Cell*  
39 *Proteomics*, 2013, **12**, 3898–3907.
- 40 11. M. A. Unger, H. P. Chou, T. Thorsen, A. Scherer, and S. R. Quake, *Science*, 2000,  
41 **288**, 113–116.
- 42 12. I. Vivanco and C. L. Sawyers, *Nat Rev Cancer*, 2002, **2**, 489–501.
- 43 13. K. M. Nicholson and N. G. Anderson, *Cellular Signalling*, 2002, **14**, 381–395.
- 44 14. B. D. Manning and L. C. Cantley, *Cell*, 2007, **129**, 1261–1274.
- 45 15. M. P. Scheid, P. A. Marignani, and J. R. Woodgett, *Molecular and Cellular Biology*,  
46 2002, **22**, 6247–6260.
- 47 16. D. D. Sarbassov, *Science*, 2005, **307**, 1098–1101.
- 48 17. J. R. Hart and P. K. Vogt, *Oncotarget*, 2011, **2**, 467–476.

- 1 18. K. S. Walker, M. Deak, A. Paterson, K. Hudson, P. Cohen, and D. R. Alessi, *Biochem.*  
2 *J.*, 1998, **331 ( Pt 1)**, 299–308.
- 3 19. D. A. Cross, D. R. Alessi, P. Cohen, M. Andjelkovich, and B. A. Hemmings, *Nature*,  
4 1995, **378**, 785–789.
- 5 20. J. McDonald and G. Whitesides, *Accounts Chem Res*, 2002, **35**, 491–499.
- 6 21. R. Gómez-Sjöberg, A. Leyrat, D. Pirone, C. Chen, and S. Quake, *Anal Chem*, 2007,  
7 **79**, 8557.
- 8 22. Q. Shi, L. Qin, W. Wei, F. Geng, R. Fan, Y. S. Shin, D. Guo, L. Hood, P. S. Mischel,  
9 and J. R. Heath, *PNAS*, 2012, **109**, 419–424.
- 10 23. F. S. O. Fritsch, C. Dusny, O. Frick, and A. Schmid, *Annu. Rev. Chem. Biomol. Eng.*,  
11 2012, **3**, 129–155.
- 12 24. C. S. Park, *Journal of Biological Chemistry*, 2003, **278**, 37064–37072.
- 13 25. S. Favelyukis, J. H. Till, and S. R. Hubbard, *Nature Structural & ...*, 2001.
- 14 26. S. Rankin and E. Rozengurt, *J Biol Chem*, 1994, **269**, 704–710.
- 15 27. H. Kato, T. N. Faria, B. Stannard, C. T. Roberts, and D. LeRoith, *J Biol Chem*, 1993,  
16 **268**, 2655–2661.
- 17 28. M. Jarvius, J. Paulsson, I. Weibrecht, K.-J. Leuchowius, A.-C. Andersson, C. Wählby,  
18 M. Gullberg, J. Botling, T. Sjöblom, B. Markova, A. Ostman, U. Landegren, and O.  
19 Söderberg, *Mol. Cell Proteomics*, 2007, **6**, 1500–1509.
- 20 29. C. Pierre-Eugene, P. Pagesy, T. T. Nguyen, M. Neuillé, G. Tschank, N. Tennagels, C.  
21 Hampe, and T. Issad, *PLoS ONE*, 2012, **7**, e41992.
- 22 30. Y. Buganim, D. A. Faddah, A. W. Cheng, E. Itskovich, S. Markoulaki, K. Ganz, S. L.  
23 Klemm, A. van Oudenaarden, and R. Jaenisch, *Cell*, 2012, **150**, 1209–1222.
- 24 31. T. Trcek, D. R. Larson, A. Moldón, C. C. Query, and R. H. Singer, *Cell*, 2011, **147**,  
25 1484–1497.
- 26 32. N. Battich, T. Stoeger, and L. Pelkmans, *Nat Meth*, 2013, **10**, 1127–1133.
- 27 33. F. Marks, U. Klingmüller, and K. Müller-Decker, 2009.
- 28 34. S. Frame and P. Cohen, *Biochem. J.*, 2001, **359**, 1–16.
- 29 35. Y. Saito, J. R. Vandenheede, and P. Cohen, *Biochem. J.*, 1994, **303**, 27–31.
- 30  
31